Astron. Astrophys. 317, 859–870 (1997)

ASTRONOMY
AND
ASTROPHYSICS

IRAS 22272+5435 – a source with 30 and 21 μm features

R. Szczerba[1,2,3], **A. Omont**[2], **K. Volk**[1], **P. Cox**[4,5], **and S. Kwok**[1]

[1] Department of Physics and Astronomy, University of Calgary, Calgary, Alberta, Canada T2N 1N4
[2] Institut d'Astrophysique de Paris, C.N.R.S., 98bis bd. Arago, F-75014 Paris, France
[3] N. Copernicus Astronomical Center, ul. Rabiańska 8, PL-87-100 Toruń, Poland
[4] Observatoire de Marseille, 2 pl. Leverrier, F-13248 Marseille Cedex 04, France
[5] Max-Planck-Institut für Radioastronomie, Postfach 2024, D-53121 Bonn, Germany

Received 31 October 1995 / Accepted 17 May 1996

Abstract. Recent observations have shown that IRAS 22272+5435, a post-AGB object with a cool central star, is one of the few sources known which displays strong 21 and 30 μm features. We present a detailed analysis of the spectral energy distribution and discuss the possible nature of the dust grains in the circumstellar envelope around this source. We find that grains of pure magnesium sulfides could be responsible for the observed 30 μm feature provided they have a high enough temperature and an appropriate broad distribution of shapes inside the shell. The absorption properties of such grains at optical and ultraviolet wavelengths are unknown, so at the present time we are unable to estimate how high a temperature they would have in the circumstellar shell; laboratory measurements of the the optical properties are needed. The 30 μm feature cannot be produced by mantles of magnesium sulfide covering an amorphous carbon core as such grains are shown to have two maxima in their absorption cross sections around a minimum at about 30 μm. Since the material(s) responsible for 21 and 30 μm features is (are) still unknown we constructed an empirical opacity function which provides a reasonable fit to the energy distribution at far-infrared wavelengths. We also show that small particles (with radii smaller than 10 Å) having properties very similar to those of PAH molecules are an indispensable part of dust around this source. For these small grains the quantum treatment of heating and cooling processes is important. Assuming that the central star of IRAS 22272+5435 is burning H quiescently in a shell, the parameters of the best fit to the energy distribution of this source indicate a stellar core mass 0.60 $M_\odot$ which is presently evolving with no (or with very little) mass loss.

Key words: stars: AGB, post-AGB – circumstellar matter – stars: individual: IRAS 22272+5435 – infrared: stars

Send offprint requests to: R. Szczerba: szczerba@ncac.torun.pl

1. Introduction

Studies of proto-planetary nebulae (PPNe) developed rapidly after the Infrared Astronomical Satellite (IRAS) mission. PPNe are objects in transition between asymptotic giant branch (AGB) stars and planetary nebulae (PNe). They are formed during evolution along the AGB when the mass of the H-rich envelope drops to very small values (about 10^{-3} $M_\odot$ for a core mass of 0.60 $M_\odot$ – see Schönberner 1983), mainly as a result of the large-scale mass loss process (nuclear reactions are less important during the formation of PNe). PPNe are very intriguing objects because of rapid changes in the stellar temperature and, consequently, in the physical conditions inside the ejected shell and the remnant stellar atmosphere. These changes could be responsible for the excitation of the 21 μm band (Kwok et al. 1989) which seems to be observed only during the post-AGB phase of evolution (although Henning et al. 1996 selected a few young stellar objects as new candidates with a 21 μm feature). Until now only nine PPNe are known (Kwok et al. 1995) to display the 21 μm emission band (Henning et al. proposed two more PPNe candidates with 21 μm features). Four of the sources known to have the 21 μm feature in their spectra were observed with the Kuiper Airborne Observatory (KAO) and were found to show a spectacular, very broad emission feature around 30 μm (Omont 1993; Cox 1993). This feature was previously known in a number of carbon-rich objects among AGB stars and PNe.

One such source is IRAS 22272+5435 (hereafter IRAS 22272) which has one of the strongest 30 μm features among the PPNe, accounting for about 20 % of its infrared bolometric luminosity (Omont et al. 1995a, b). IRAS 22272+5435 (known also as BD+54°2787 = HD 235858 = SAO 34504) is a source which was initially classified as an O-rich star because the shape of its IRAS Low Resolution Spectrum (LRS) suggests the presence of silicate absorption features at about 9.7 and 18 μm (see e.g. Pottasch & Parthasarathy 1988). The detection of CO emission (Zuckerman et al. 1986) followed by the re-detection of CO and other carbon-bearing molecules such as HCN, CS and CN (see Lindqvist et al. 1988) did not change the classification of IRAS 22272. In his paper devoted to the

21 μm feature, Kwok et al. (1989) called attention to the extreme carbon richness of the all 21 μm sources and refers to the observations later presented in Hrivnak & Kwok (1991) where they confirmed the C-richness of IRAS 22272 by detection of strong optical absorption bands of C_3 and C_2 (see also Hrivnak 1995). Further the comparison of the LRS spectrum of IRAS 22272 with those of IRAS 07134+1005 and IRAS 23304+6147 showed that the features in the LRS spectrum are not due to silicates, although they also are not typical of carbon-rich sources. Measurements of a large ratio of the millimeter HCN/CO line intensities (Omont et al. 1993 concluded that $CO(1 \rightarrow 0)/HCN < 5$ and/or $CO(2 \rightarrow 1)/HCN < 12$ seem to be a good indicator of C-richness and in the case of IRAS 22272 they found $CO(1 \rightarrow 0)/HCN = 3.9$ and $CO(2 \rightarrow 1)/HCN = 4.8$) and the detection of infrared (IR) features at 3.3, 3.4, 6.2, 6.9, 7.7 and 11.3 μm (Buss et al. 1990; Geballe et al. 1992; Buss et al. 1993) attributed to a mixture of polycyclic aromatic hydrocarbons (PAHs) and some sort of carbon clusters reinforced the conclusion that IRAS 22272 is C-rich. Also, recent analysis of a high-resolution optical spectrum for IRAS 22272 by Začs et al. (1995) clearly indicates the star is extremely carbon-rich (they estimated $C/O \sim 12$).

The main aim of this paper is to discuss the properties of the dust grains which could account for the spectral energy distribution (SED) of IRAS 22272 together with the unusual emission features observed in its spectrum. The paper is organized as follows. First, we describe the computer code and the input parameters which were used to study the energy distribution in post-AGB objects (Sect. 2). Next we discuss the dust optical properties which are adopted in the present modeling of IRAS 22272: the types of dust considered include PAHs, amorphous carbon, magnesium sulfides and an empirical opacity function which accounts for the 21 and 30 μm features (Sect. 3). In the subsequent Sects. (4 and 5), we present the results of the model and discuss in detail the implications of the derived parameters. Conclusions are given in Sect. 6.

2. Description of the computer code

A detailed description of the basic method used in the code and its equations is given by Yorke (1980a, 1980b). Briefly, the frequency-dependent radiative transfer equations are solved under the assumption of spherically-symmetric geometry simultaneously with the thermal balance equation for a dusty envelope. However, significant modifications to the original code have been made. First, we have changed the method of integration of the ray equations by carrying out the solution twice and taking the geometrical mean of the resulting specific intensities. As in the original version of the code, we assume that source function (S_ν) is constant on the interval from radial grid point $r_{\rm j}$ to $r_{\rm j-1}$, but now the ray equations are solved first with the values $S_\nu(r_{\rm j})$ and then with the values $S_\nu(r_{\rm j-1})$. The same method of integration was applied in the case of the optical depth (τ_ν), treating now the extinction coefficient ($\alpha_{\rm ext,\,\nu}$), which is sum of the absorption and scattering coefficients, in the same way as the source function above. Such an approach significantly increases the accuracy of the ray equation integration.

We have also increased the number of impact parameters between stellar surface and the first radial grid point (see Fig. 4 in Yorke 1980b). In the original version of the code only one impact parameter (just missing the stellar surface) was used. Increasing in the number of rays within the inner radius of the dust shell is crucial in the study of detached dusty shells such as investigated in this paper because the inner radius of the shell ($r_{\rm in}$) is far away from the stellar surface.

Next, we have changed the code by introducing a grain size distribution for each of the two dust components. In the present version we have introduced a size distribution described by a power law index (p) for all dust radii in the range from a minimum radius (a_-) to a maximum radius (a_+). In such a case the source function is given by (compare this to S_ν given by Eq. 7 of Yorke 1980b):

$$S_\nu(r) = \frac{\sum_{i=1}^{2} X_i(r) \left[\int_{a_-}^{a_+} C^i_{\rm abs,\,\nu}(a)\, B_\nu \left[T^i_{\rm d}(r,a)\right]\, a^{-p}\, da \right]}{\alpha_{\rm ext,\,\nu}} + \frac{\alpha_{\rm sca,\,\nu}\, J_\nu(r)}{\alpha_{\rm ext,\,\nu}}. \quad (1)$$

Here the thermal emission by dust grains of i-th type with size a at a given distance r from the central source, with a temperature $T^i_{\rm d}(r,a)$ found from the solution of the thermal balance equation, is characterized by the Planck function $B_\nu\left[T^i_{\rm d}(r,a)\right]$ and the mean intensity of the radiation field is represented by $J_\nu(r)$. Symbols without index i are sums of the corresponding quantities over dust components. The extinction coefficient is defined as: $\alpha^i_{\rm ext,\,\nu}(r,a) = n_i(r,a)\, C^i_{\rm ext,\,\nu}(a)$, where $C^i_{\rm ext,\,\nu}(a)$ is the extinction cross section (sum of the absorption and scattering cross sections), and the size distribution of such particles is described by $n_i(r,a) = X_i(r)\, a^{-p}$ where $X_i(r)$ is a normalization constant given by

$$X_i(r) = \frac{3\,(4-p)\,\psi_i\,\rho_{\rm gas}(r)}{4\,\pi\,\left[(a_+)^{4-p} - (a_-)^{4-p}\right]\,\rho_i} \qquad \text{for} \qquad p \neq 4.$$

Here ψ_i is dust-to-gas ratio, $\rho_{\rm gas}(r)$ is gas density at distance r from the star and ρ_i is the specific density of the material forming the i-th type of dust grain.

Finally, we have introduced temperature calculations of very small dust particles using the quantum approach. In the case of very small dust particles the absorption of an individual energetic photon produces a significant over-heating yielding a temperature much higher than the equilibrium value and, in consequence, the equilibrium temperature calculation gives a poor approximation to the grain emission. A set of temperature bins is defined, and transition rates into and out of each bin are calculated for the local radiation field, from which the temperature probability distribution can be calculated. The treatment follows that of Guhathakurta & Draine (1989) with the exception that we only consider the quantum effects of the radiation field and neglect those of electron collisions. In the case of post-AGB

objects electron densities are negligible and such an approach seems to be justified.

The source function in this case (dust size distribution together with non-equilibrium heating) was constructed by dividing the integral over dust sizes in Eq. (1) into two components:

$$\int_{a_-}^{a_{\rm qh}(r)} C^i_{{\rm abs},\,\nu}(a) \left\{ \sum_k P_k \left[T^i_{\rm d}(r,a)\right] B_\nu \left[T^i_{\rm d}(r,a)\right] \right\} a^{-p}\, da$$

$$+ \int_{a_{\rm qh}(r)}^{a_+} C^i_{{\rm abs},\,\nu}(a)\, B_\nu \left[T^i_{\rm d}(r,a)\right]\, a^{-p}\, da. \qquad (2)$$

Here $a_{\rm qh}(r)$ is the maximum size of dust particles for which quantum effects are still important. This size could be different for each of the dust components and is a strong function of the local radiation field. $\mathrm{P}_k\left[T^i_{\rm d}(r,a)\right]$ is the probability ($\sum\limits_k P_k\left[T^i_{\rm d}(r,a)\right] = 1$) that a dust particle has a temperature $\mathrm{T}^i_{\rm d}(r,a)$. The index k represents the number of temperature bins and thermal emission from dust grains for which quantum processes are important is given by:

$$C^i_{{\rm abs},\,\nu}(a) \left\{ \sum_k P_k[T^i_{\rm d}(r,a)] B_\nu[T^i_{\rm d}(r,a)] \right\}.$$

Tests of our code have been performed to check consistency with other existing codes. Excluding quantum treatment of dust temperature calculations and restricting the distribution of grain sizes to the single size, we have checked that our code reproduce exactly results of the DUSTCD code (see e.g. Leung 1975, 1976 and Egan et al. 1988).

We have also checked quantum heating calculations by comparing our model results with those published by Siebenmorgen et al. (1992) – their Figs. 1a and 1b. We were able to closely reproduce their probability density (defined as the probability that dust particle temperature belongs to the interval $[T_{\rm d}, T_{\rm d}+1]$ – a somewhat different definition than the one adopted in this paper) and their results for the emission of small graphite grains.

3. Dust optical properties

3.1. Infrared emission bands and the underlying infrared continuum

To account for the presence of the infrared emission features in the spectrum of IRAS 22272, we have included in our code PAH grains, assuming that PAHs have the same enthalpy as graphite grains (see Siebenmorgen & Krügel 1992) – knowledge of the enthalpy is required during non-equilibrium temperature calculations. The cross-sections for the PAH grains are based upon the analytical formulae given by Desert et al. (1990). Some changes have been made in the discrete PAH feature strengths following the values in Schutte et al. (1993) because their values for the bands near 11 μm seem to be better. Some plateau shapes have also been added to the cross-section values based upon

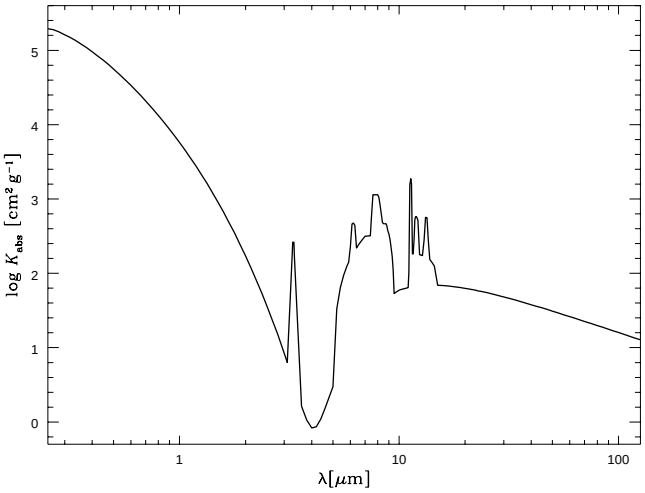

Fig. 1. Adopted mass absorption coefficient of PAH grains with radius of 10 Å .

the observations of Bregman et al. (1989). In addition the equations from Desert et al., which were only intended to apply for wavelengths greater than the Lyman limit, were not used at wavelengths less than 912 Å as they give values that continue to increase rapidly as the wavelength decreases. Instead a linear extrapolation of the values near the Lyman limit was used for the shorter wavelength cross-sections, producing values that do not rise very rapidly as the wavelength decreases. In addition the sharp cut-off of the optical cross-section at 8000 Å in the paper of Desert et al. has been replaced by an exponential decline with increasing wavelength that starts at 2500 Å and which is set to produce a feature to continuum ratio of 100 at 3.3 μm. This was done in part to avoid discontinuities in the opacity values and in part to allow the possibility of modeling the unusual red emission seen in a few reflection nebulae that have strong PAHs emission. It should be noted that the long wavelength opacity function for the PAH grains is poorly known, and therefore the infrared emission from the PAH grains is suspect aside from the discrete features. This is not a problem in practical situations however, because the PAH grains are not observed to occur without other forms of dust which dominate the emission except at the discrete PAH features.

The PAH grain cross-sections were calculated for 12 logarithmically spaced grain radii from 3.5 Å up to 50 Å and, as an example, the adopted mass absorption coefficient ($K_{\rm abs}$) for PAHs of 10 Å radius ($\sim$ 120 C atoms) in the wavelength range from about 0.25 to 125 μm (in total, 256 λ's from 100 Å up to 3000 μm were used in the radiative transfer calculations) is shown in Fig. 1.

As the other form of carbon-based dust appearing together with the PAHs we have chosen amorphous carbon of type AC (soot produced by striking an arc between two amorphous carbon electrodes in a controlled argon atmosphere – see Bussoletti et al. 1987 for details). Using real and imaginary parts of the complex refractive index computed for AC dust by Rouleau & Martin (1991) we have calculated absorption and scattering

efficiencies on the basis of Mie theory for 30 logarithmically spaced grain radii from 10 Å up to 1 μm. Finally, we have assumed that the dust responsible for the infrared emission bands and the infrared continuum emission in post-AGB objects is made of: PAHs for 5 Å $< a <$ 10 Å, amorphous carbon grains for $a >$ 50 Å and dust with an opacity obtained from averaging of the absorption efficiences for PAH and AC grains according to the formula

$$Q_{\mathrm{abs},\,\nu} = \mathrm{f} \cdot Q^{\mathrm{PAH}}_{\mathrm{abs},\,\nu}(a) + (1 - \mathrm{f}) \cdot Q^{\mathrm{AC}}_{\mathrm{abs},\,\nu}(a),$$

for grain sizes between 10 and 50 Å. Here f = 1 for a = 10 Å and f = 0 for a = 50 Å. The last form of dust was introduced to keep continuous distribution of dust grain sizes and to fill the gap between properties of large carbon-bearing molecules and small grains.

We performed a few numerical trials trying to incorporate graphite grains into our model (see Laor & Draine 1993 for the most recent source of the optical opacity data for graphite). However, we found that the absorption efficiency of graphite is too steep in the far-infrared (FIR) and also in the mid-infrared (MIR). In the FIR range of the spectrum our model is not able to predict enough flux at 100 μm. Only increasing the number of cold graphite grains (e.g. by assumption that $\dot{M}$ decreased significantly during the formation of the shell) could explain the observed far-infrared emission. On the other hand, if we try to match an observed continuum level at around 18-19 μm the predicted emission at near-infrared wavelengths is too high. This seems to suggest that the dust around the C-rich post-AGB objects is amorphous rather than graphitic in form.

3.2. Features around 21 and 30 μm

IRAS 22272+5435 is one of the four post-AGB sources where the 21 μm feature was discovered by analysis of the IRAS LRS database (Kwok et al. 1989). Subsequent measurements made on the KAO have detected a prominent emission band around 30 μm in four 21 μm sources including IRAS 22272 (Omont et al. 1995b). It has been proposed that the 30 μm emission band, which is also detected in C-rich AGB stars and post-AGB stars including planetary nebulae (see Omont et al. 1995b and references therein), could be due to solid magnesium sulfide, MgS (Goebel & Moseley 1985). Recently, Begemann et al. (1994) tabulated the optical constants of Mg-Fe sulfides as derived from laboratory measurements in the wavelength range from 10 to 500 μm. In Fig. 2 we display the mass absorption coefficient for a mixture composed of 90 % MgS and 10 % FeS as derived by us from the optical constants of Begemann et al. (1994). The dotted line shows the results based on Mie theory and the short dashed line the mass absorption coefficients for a continuous distribution of ellipsoids (hereafter CDE: see Bohren & Huffman 1983). As compared to the Mie theory, the CDE computations predict a feature which is much broader with a peak shifted towards longer wavelengths at about 35 μm. We note that the lack of the refractive index data for sulfides in the short wavelength range prevents detailed quantitative modeling. An empirical approach to estimate their FIR emission will be given in Sect. 4.

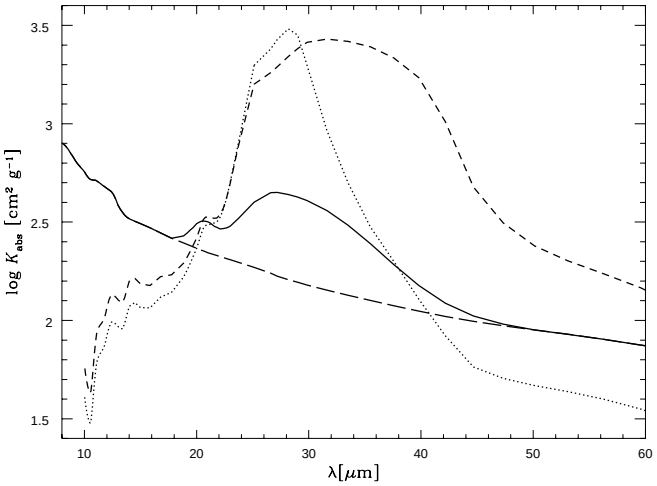

Fig. 2. Mass absorption coefficients for: empirical opacity function used in modeling of IRAS 22272 (solid line); MgS-FeS mixture computed on the basis of the Mie theory (dotted line); the same mixture of sulfides but now computed in the CDE approximation (short dashed line). Long dashed line represents underlying continuum level of pure AC grain with radius of 0.1 μm.

As far as 21 μm band is concerned the problem of the identity of the emitter remains unknown. Currently, the most accepted materials responsible for this feature in C-rich PPNe seem to be PAHs or PAH clusters (a much wider discussion of the possible carriers of the 21 μm emission band as well as physical and chemical conditions necessary for their production can be found in recent papers by Kwok et al. 1995, Omont et al. 1995b and Henning et al. 1996). While Kwok et al. and Omont et al. suggested that 21 μm feature is present (excited) only during a short PPNe phase of evolution, Hening et al. found that this band is observed in some young stellar objects as well. It could mean that the physical and chemical conditions which produce the carrier of the 21 μm feature in the circumstellar environment (e.g. high speed molecular stellar winds and/or high velocity streaming of grains through gas) are similar during these two different stages of stellar evolution.

Since the real carriers of 21 and 30 μm bands are still not identified (and therefore their optical properties are unknown), we adopted an empirical opacity function (EOF) which takes into account both these features to perform a quantitative modeling of the energy distribution. This empirical opacity was defined by adding features onto the mass absorption coefficient for AC amorphous carbon grains with radius of 0.1 μm. In principle, K_{abs} is constant in the mid- and far-infrared (i.e. Q_{abs}/a is independent of a), so the exact choice of the AC grain size is unimportant. Also, scattering efficiencies are small at these wavelengths, so changes were made only to the absorption opacity. For the 21 μm emission band we approximated its shape by a gaussian fit with a centre wavelength of 20.6 μm and a width at half maximum of 1.5 μm as determined from the source IRAS 07134+1005 which has the strongest known 21 μm fea-

ture (Kwok et al. 1989). For the 30 μm emission band shape a simple gaussian shape is inadequate because the feature is asymmetric with the short-wavelength side of the peak significantly sharper than the long-wavelength side. Therefore we fitted the 30 μm band with two half-gaussians instead, having the same central wavelength and peak strength but different widths. The values of these parameters as determined from modelling of IRAS 22272 are: 27.2 μm for the central wavelength and 4.0 and 9.0 μm for the widths at half maximum. It was necessary to perform several radiative transfer calculations to find out the values of the feature parameters that gave a reasonable fit.

The resulting opacity function including the 21 and 30 μm features and the mass absorption coefficient of AC amorphous carbon is displayed in Fig. 2 as a solid line. For comparison purposes, Fig. 2 also shows the underlying continuum due to pure AC grains (long-dashed line). We note that $K_{\rm abs}$ for the EOF is much smaller at 30 μm as compared to that for a mixture of Mg and Fe sulfides. However, this is not crucial since the empirical opacity was added to the opacities of the amorphous carbon grains implying that the strength of the EOF is determined by the required amount of the AC providing the best fit to the infrared continuum emission. The shape of the opacity function is much more important. It is clear from Fig. 2, that long-wavelength side of the EOF lies in between $K_{\rm abs}$ for the mixture of sulfides calculated from the Mie theory (spherical grains) and from CDE approximation (distribution of ellipsoids).

The strong dependence of the MgS absorption properties on the shape of the grains is a consequence of the very large values for the refractive index (see Begemann et al. 1994). Because our opacity function gives an excellent fit to the observed energy distribution of IRAS 22272 (see below) we can conclude that if sulfides are indeed responsible for the observed 30 μm feature then the shape of these grains is quite important. A simple variation in the distribution of the dust grain shapes could change the long-wavelength shape of this feature. Finally, it is worth noting that the short-wavelength parts are quite similar for all of the opacities used for modelling of the 30 μm emission band.

3.3. Carbon grains coated by sulfide particles

In order to identify the carrier of the 30 μm feature, we have tested the possibility of MgS condensing on the surface of AC grains. The material responsible for the feature in IRAS 22272 must absorb as much as 20 % of the heating ultraviolet (UV) and visual radiation which is absorbed by dust. Therefore, the material must either have sufficient absorption cross section or exist as a thin mantle on grains of sufficient cross section (Nuth et al. 1985). To calculate the optical properties of spherical AC (core) grains coated by MgS (coat), we used the method and the computer code described in Bohren and Huffman (1983). The thickness of the coating layers was computed assuming that all available sulphur (n(S)/n(H) $\approx$ 10^{-5}, e.g. Aller & Czyzak 1983) is tied up in Mg–Fe sulfides composed of 90 % of MgS and 10 % of FeS and that all the coating material is distributed proportionally to the surface areas of the AC grains.

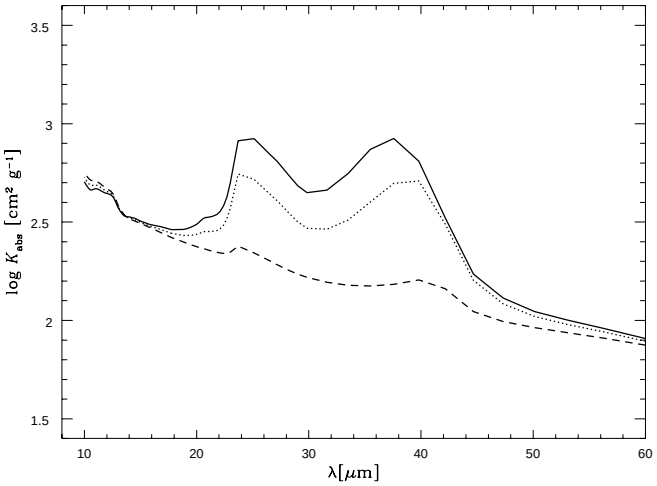

Fig. 3. Mass absorption coefficient for AC grains coated with mixture composed of 90 % MgS and 10 % FeS: solid line ($a_{\rm core}$ = 50 and $a_{\rm coat}$ = 55.5Å); dotted line ($a_{\rm core}$ = 0.01 and $a_{\rm coat}$ = 0.0106 μm); dashed line ($a_{\rm core}$ = 0.1 and $a_{\rm coat}$ = 0.1006 μm).

One of the consequence of such an assumption is that smaller AC grains will have thicker mantles (relative to their radius). For the parameters describing the dust size distribution of pure AC grains in our model of IRAS 22272 (i.e., a_- = 50 Å, a_+ = 0.25 μm, p = 3.5 [1] and dust-to-gas ratio Ψ = 0.005), we obtained radii of the coated grains up to 11 % larger than the radii of the core grains in the case of the smallest (50 Å) AC particles and only 0.3 % greater in the case of the largest (0.25 μm) ones (for larger Ψ the ratio of the radii would be even smaller).

In Fig. 3 we present the mass absorption coefficient of the homogeneous AC spheres of different radii coated with a homogeneous layer of Mg–Fe sulfides as computed under the above assumptions. The scale and the range of the $K_{\rm abs}$ and wavelengths are the same as in Fig. 2 to allow a direct comparison between the expected features. As one can see for thin sulfide mantles ($a_{\rm coated\ grain}/a_{\rm core}$ < 1.2), which are required because of the sulphur abundance constraints, we obtain two peaks at about 24 and 38 μm with a broad minimum around 28–32 μm.

[1] We have assumed that the size distribution of amorphous carbon grains follows that for the interstellar medium (Mathis et al. 1977). However, to explain SEDs of some other sources with 21 and/or 30 μm features (Szczerba et al. 1996a) it was necessary to increase number of small particles by increase of the power law index p. This is in agreement with theoretical calculations of Dominik et al. (1993) which show that the size distribution of dust particles formed in an outflow from a star consists mostly of small particles. On the other hand, these calculations (see also Jura 1994) suggest that in circumstellar envelopes the dust size distribution could have a tail composed of dust grains with larger sizes than the adopted upper limit of 0.25 μm. However, modelling of SEDs is not sensitive to the upper limit of the size distribution since only a very small fraction of dust mass is contained in particles with large radii. Here we do not study the effect of larger grains leaving the problem to the moment when more appropriate observational (e.g. polarization) data will be available.

Since all the conditions (described in Appendix B in Bohren & Huffman 1983) which are required for the code to work properly are fulfilled these features are believed to be real. Similar results were obtained by B. Glaccum (private communication). Glaccum also tested the case of the core-mantle spheroidal grains, in the Rayleigh limit, and found that for thin mantles the peaks do not really shift in frequency, but are approximately independent of the shape of the grains. The two peaks can be interpreted as the interface modes at the AC/sulfide and sulfide/vacuum interfaces. This interpretation is confirmed by analysis of the polarizability of small coated spheres, which shows that the calculated peaks occur at the positions where conditions for singularities of the polarizability are the best fulfilled (Ossenkopf, private communication).

On the other hand, for thick MgS–FeS mantles on the AC core ($a_{\rm coated\ grain}/a_{\rm core} > 1.4$) the feature is close to the observed one, but one would have a relatively small number of grains with thick mantles and most grains would be uncoated due to the limited amount of sulphur available. We did not perform radiative transfer calculations for the case of thick mantles for two further reasons: first it is not clear how to define populations of coated and uncoated grains, and, second it is not exactly known how sulfides condense. During condensation on carbon grains other materials (such as SiC) could condense at the same time so that the mantles formed need not necessarily be homogeneous. On the other hand, when condensation on AC grains is likely a separate MgS dust component seems to be possible as well.

4. Analysis of the spectral energy distribution

In Fig. 4 we have plotted available observational data for IRAS 22272+5435. Spectroscopic data plotted (shown by thin continuous lines) include the KAO spectrum in the range 16–49 μm (Omont et al. 1995b); averaged IRAS LRS spectrum (7.5–23 μm) obtained from the University of Calgary IRAS Data Analysis Facility (see details of the processing procedure in Volk et al. 1991); UKIRT spectrum from 32-channel Cooled Grating Spectrometer 3 (CGS3) kindly provided by K. Justtanont (from Justtanont et al. 1996) in the ranges from 7.6 to 13 and from 17.2 to 23.6 μm; MIR spectrum (4.8 – 13.1 μm) from Buss et al. (1990); near-infrared (NIR) spectra (2.82 – 3.72 μm) from Buss et al. (1990) and another NIR spectrum (3.15 – 3.66 μm) from Geballe et al. (1992). Photometric data shown in this figure include: two sets of photometric data at UV and visual wavelengths (filled circles or filled squares) together with estimated errors from Hrivnak & Kwok (1991) – these data are connected by thin solid lines to show more clearly the possible variations in the central star fluxes; three sets of the NIR photometry at J, H, K, L and M bands (also with estimated errors) from Manchado et al. 1989 (triangles), van der Veen et al. 1989 (squares) and from Hrivnak & Kwok 1991 (circles); IRAS Point Source Catalogue (PSC) fluxes (filled circles) together with errors at 12, 25, 60 and 100 μm (the colour corrected fluxes are represented by open symbols – see Kwok et al. 1986, for details concerning the colour-correction procedure applied); in addition, a flux measured by Walmsley et al. (1991) at 1.3 mm together with their estimated error is plotted as a filled circle.

In Fig. 4 we also present two sets of photometry (from B to M bands) corrected for interstellar extinction according to the average extinction law of Cardelli et al. (1989), assuming the total extinction at V of 1.0 or 2.0 magnitudes and plotting only the smallest and largest values of the corrected fluxes for a given band. This estimate of the total extinction was inferred from Fig. 6o (304) of Neckel & Klare (1980). The total extinction in the direction of this object shows some scatter but is almost independent of distance for $d > 1$ kpc. During modelling we tried to arrange that our model energy distribution, when normalized to the NIR data, fell in between the two sets of corrected fluxes. In this way we have taken into account the effect of the interstellar extinction. This is important for the determination of the star luminosity, or more exactly for L/d^2. Without taking into account the interstellar extinction, the derived L/d^2 value would be lower.

In spite of the possible variability of the source in the visible and UV (Hrivnak & Kwok 1991), all photometric measurements in the NIR seem to be in agreement with each other (within the estimated observational errors) and agree with the available NIR and MIR spectroscopy. This is in agreement with the variability index (only 3 % over a 6 month interval) assigned to the IRAS data. There is also an excellent agreement between the KAO observations and the IRAS fluxes: integrating the KAO spectrum over the profile of the 25 μm IRAS band yields a flux of 295 Jy to be compared to the 25 μm PSC flux of 302 Jy. A similar good agreement is found between the KAO and LRS spectra in the region where the data overlap. However, the integration of the LRS spectrum over the instrumental profile of the 12 μm IRAS band gave only 64 Jy, while PSC flux at this wavelength is about 16 % larger (74 Jy). This discrepancy seems to be produced by too low values of the fluxes in the short-wavelength part of the LRS spectrum. Two other spectroscopic measurements in the MIR region are in excellent agreement and show higher flux levels than LRS. Replacing, short-wavelength part of the LRS spectrum by data from Buss et al. (1990) results in a flux of 70 Jy – very close to the PSC flux at 12 μm. As far as long-wavelength band of CGS3 data is concerned, we can see that these values are about 10 % higher than the KAO and LRS spectra, both of which agree very well with the PSC flux at 25 μm.

Adopting a dust mixture made of PAHs, AC grains and including the empirical opacity function which was discussed in Sect. 3, we derived the fit to the spectral energy distribution of IRAS 22272 shown in Fig. 4 by the heavy solid line (as one can see our model is able to explain quite well almost all important aspects of the observed SED). The dashed line with arrow indicates the beam effect of the IRAM observations at 1.3 mm (HPBW of the telescope was $11''$ – see Walmsley et al. 1991). Our model predicts a flux density (21.5 mJy) which is consistent with the flux density observed by Walmsley et al. (16.5 ± 4.3 mJy). The small difference could be easily explained by slightly different slope of dust optical properties at sub-millimeter wavelengths. The thin long-dashed line

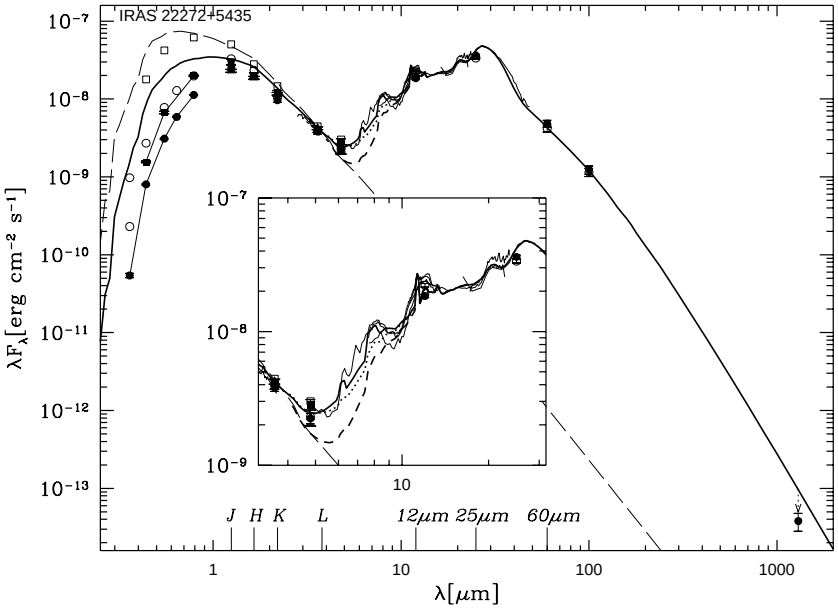

Fig. 4. Fit to the spectral energy distribution of IRAS 22272 obtained with dust properties described in Sect. 3, taking into account quantum heating effects (heavy solid line). Thin long-dashed line shows the input energy distribution of the central star, taken to radiate according to a model atmosphere calculations for log(g) = 0.5 and $T_{\rm eff}$ = 5300 K. The inset shows MIR part of the spectrum in more detail. The solid line represents our best fit, the dotted line shows the fit which was obtained assuming thermal equilibrium for all dust particles, while heavy dashed line shows the fit where, in addition, hotter dust has been neglected (see text for details). Presented photometry (filled symbols from B to M band) is corrected for interstellar extinction assuming the total extinction at V of 1.0 or 2.0 magnitudes and plotted as open symbols. The dashed line with arrow indicate the beam effect of the IRAM observations at 1.3 mm. For more details concerning observational data shown in the figure see text.

represents the input energy distribution of the central star for log(g) = 0.5 and $T_{\rm eff}$ = 5300 K according to model atmosphere calculations by Kurucz (private communication). The inset in this figure shows MIR part of the spectrum in some more details. The solid line represents our best fit which takes also into account quantum heating effects. The dotted line plotted from 4 to 11 μm shows the fit which was obtained when no quantum treatment of small grain heating was included. As we can see the quantum heating effects are necessary to explain the presence of the emission features at 6.2, 7.7 and 8.6 μm. But otherwise the quantum effects appear to have only a relatively moderate role in producing the spectrum of IRAS 22272. We note that in other sources displaying the 21 and/or 30 μm features this is not the case and that quantum effects are much more important (a detailed analysis of these sources will appear elsewhere – Szczerba et al. 1996a, see also Szczerba et al. 1996b). The short-dashed line presents the effect of neglecting the quantum treatment for the dust temperature and supposing that there is no hot dust present between the star and the main detached shell. The parameters of the model fit shown in Fig. 4 are listed in Table 1.

As we can see from Fig. 4 a small amount of hot dust seems to be necessary (about 6.75 10^{-7} $M_\odot$ which corresponds to gas mass of 1.35 10^{-4} $M_\odot$ if $\Psi = 0.005$ is adopted) to obtain a good fit to the observed SED in the NIR. It can be interpreted as an indication that the mass loss on the AGB diminished gradually rather than stopping abruptly. Of course, another explanation is that a process of new mass loss has just started. However, in our model the inner radius of hot dust is 7.8 10^{-4} pc and the average dust temperature at this radius is only about 660 K so it is rather difficult to understand why and how dust could condense at such large distance (about 300 stellar radii) where the gas density is rather low, probably too low to start process of the new dust condensation. Any attempt to include much hotter dust ($T_{\rm d}$ above 1000 K) in our model resulted in too much emission predicted in the NIR. Therefore, we favor a scenario in which the mass loss process, which is inseparably connected to dust formation, stopped about 50–100 years ago after a quite long period of decline.

Table 1. Model parameters for IRAS 22272+5435.

parameter	value
$T_{\rm eff}$	5300 K
log ($L_{\rm star}$ [$L_\odot$])	3.92
d	1.67 kpc
$R_{\rm out}$	0.5 pc
$V_{\rm exp}$	10 km s^{-1}
$R_{\rm in}$(hot dust shell)	7.8 10^{-4} pc
$\overline{T}_{\rm d}$[$R_{\rm in}$(hot dust shell)]	660 K
$\rho_{\rm gas}$ (hot dust shell)	$\sim r^{-2.0}$
$\dot{M}_{\rm post-AGB}$	2.0 10^{-7} $M_\odot$ yr^{-1}
$R_{\rm in}$(main shell)	7.67 10^{-3} pc
$\overline{T}_{\rm d}$[$R_{\rm in}$(main shell)]	230 K
$\rho_{\rm gas}$ (main shell)	$\sim r^{-2.6}$
$\dot{M}^{\rm min}_{\rm AGB}$	4.70 10^{-6} $M_\odot$ yr^{-1}
$\dot{M}^{\rm max}_{\rm AGB}$	5.76 10^{-5} $M_\odot$ yr^{-1}
a_-	5Å
a_+	0.25 μm
p	3.5
$t_{\rm dyn}$	750 yr
$M_{\rm dust}$	0.0023 $M_\odot$

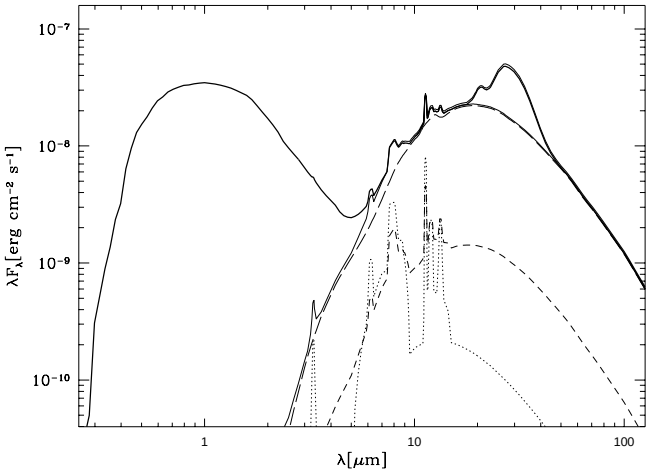

Fig. 5. Estimation of the IR continuum level below 21 and 30 μm bands (thin solid line: see text for more details) which is sum of three components: PAHs with radii from 5 to 10 Å (dotted line); mixture of PAH and pure AC grains (EOF has been neglected) for radii from 10 to 50 Å (dashed line); pure AC grains with radii from 50 Å to 0.25 μm (long-dashed line). Heavy solid line shows the best fit (the same as in Fig. 4), while thin solid line with features at 21 and 30 μm shows IR emission as estimated assuming that shell is optically thin.

To estimate the infrared emission underlying the 21 and 30 μm features, we assumed that shell is optically thin in the wavelength range of interest, i.e. from 18 to 50 μm. Taking into account PAHs and pure AC grains only (no EOF) we used equilibrium temperatures or (in the cases where quantum effects are important) probabilities that the dust particles are at a given temperatures, as found from the solutions of detailed radiative transfer calculations for dust with EOF, to estimate the infrared flux outgoing from the shell.

Fig. 5 presents the model results (without the observational data and now for λ less than about 200 μm) and shows the estimated IR continuum level underlying the 21 and 30 μm bands (thin solid line) together with its decomposition into the contributions of the different types of dust grains: PAHs with radii from 5 to 10 Å (dotted line), mixture of PAH and pure AC grains for radii from 10 to 50 Å (short-dashed line) and pure AC grains with radii from 50 Å to 0.25 μm (long-dashed line). The thin solid line with features at 21 and 30 μm presents the results for dust with the EOF assuming also that dust shell is optically thin in the MIR and FIR, while the heavy solid line shows the same fit as in Fig. 4. As can be seen, the assumption that the shell is optically thin in the mid- and far-infrared is quite good (the thin solid line agrees quite well with the heavy one). The difference between the approximated flux and the flux of the best fit model is between 3.6 and 4.6 %. Taking into account the estimated continuum level (lowered by 4 % for the above reason) and assuming that 21 μm feature extends from 18 to 22 μm while the 30 μm feature extends from 22 up to 48 μm, we estimate that the energy emitted in the 21 μm band represents 2.3 % of the total infrared emission (1470 $L_\odot$ in between 5 and 300 μm adopting a distance to the source of 1 kpc). The energy in the 30 μm band is estimated to account for as much as 24 % of the total IR emission.

As mentioned before, the available opacity data for MgS grains does not provide sufficient information to carry out detailed quantitative modeling. However, we can estimate the IR emission due to sulfides by assuming that the shell is optically thin and that quantum effects are not important near 30 μm (both assumptions are fulfilled quite well - see Figs. 4 and 5).

For sulfide dust grains with a size distribution given by $n(r,a) = X(r)\,a^{-p}$, which are in thermal equilibrium inside an optically thin shell, we can write the contribution to infrared energy emitted per cubic centimeter as follows

$$P_\nu(r) = \frac{16}{3}\,\pi^2\,X(r)\,\rho \int_{a_-}^{a_+} a^{3-p}\,B_\nu[T_{\rm d}(r,a)]\,K_{{\rm abs},\,\nu}(a)\,da,$$

where ρ means dust specific density. The mass absorption coefficient for sulfides in the far-infrared is not a function of dust size, so the only hidden dependence on a in the integral above is the dependence of the dust temperature on the size (in principle, dust particles of different sizes will have different temperatures because their UV and visual absorption properties could differ). We have no laboratory measurements of the optical properties of sulfides for wavelengths shorter than 10 μm so we cannot estimate their temperatures. Therefore, for simplicity, we assumed that at a given distance r from the central source grains of all sizes have the same temperature. Then the volume emissivity is simply given by:

$$P_\nu(r) = 4\,\pi\,K_{{\rm abs},\,\nu}\,B_\nu[T_{\rm d}(r)]\,\rho_{\rm sulf}(r),$$

where $\rho_{\rm sulf}(r)$ is the density of sulfide grains at distance r. In the case of post-AGB objects maximum density of sulfides is determined by the abundance of sulphur (n(S)/n(H) $\approx 10^{-5}$ – Aller & Czyzak 1983). Therefore, we can represent the density of sulfides by the density of gas and the amount of sulphur which is tied up in it:

$$\rho_{\rm sulf}(r) = 0.71\,\rho_{\rm gas}(r)\,(88 - 32\,\alpha)\,n({\rm S})/n({\rm H}).$$

where the factor 0.71 assumes a ratio n(He)/n(H) of 0.1 and α represents the fraction of MgS in the MgS–FeS mixture (α = 0.9 was taken). Finally, with some simplifying assumptions, we obtain a formula for the volume emissivity of sulfides with the only one unknown, in fact the most important quantity, which is the dust temperature itself.

In Fig. 6 we show the highest dust equilibrium temperature distribution as obtained from the modeling of IRAS 22272 for PAH molecules with size a = 10 Å (solid line) as well as the lowest one obtained for AC and EOF grain with size of 0.01 μm (dotted line). Spikes seen on these curves, at the radius where hot dust shell and main dust shell join each other, are results of different densities in the two regions (see Table 1 for details). Now, assuming that one of these temperature distributions applies to sulfides, we can estimate the total IR emission of the MgS–FeS grains, by integrating the emissivity estimated above over the volume of the shell.

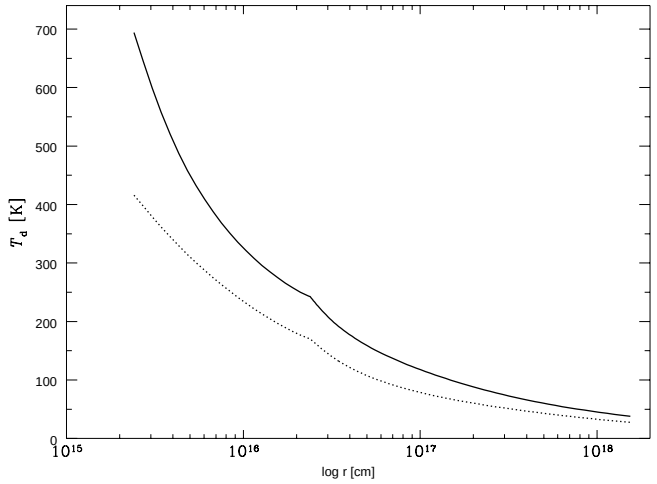

Fig. 6. Distribution of equilibrium dust temperature inside shell model of IRAS 22272 for PAH grain with radius of 10 Å (solid line) and for AC with EOF grain of 0.01 μm size (dotted line).

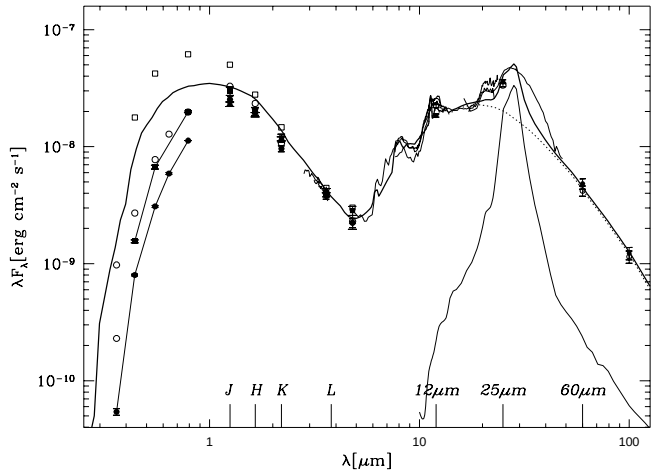

Fig. 7. Fit (heavy solid line) to the spectral energy distribution of IRAS 22272 obtained by summation of IR emission by spherically symmetric sulfide grains with the highest temperature distribution found in our model (thin solid line) and the IR continuum level (dashed line). For details concerning observational data see Sect. 4.

To compute the total IR energy emitted by the shell we took into account the IR continuum level under the 30 μm feature (see thin solid line in Fig. 5) and added to it the contribution from the MgS–FeS mixture. Trying to find a reasonable fit we were able to estimate the amount of sulphur which is tied up in sulfides. In Figs. 7 and 8, we show the fits obtained for the highest dust temperature distribution found in our model assuming that the MgS and FeS grains are spherical or that their optical properties are such as computed from CDE approximation, respectively. Both fits require n(S)/n(H) = 4 10^{-6}, well below the abundance of sulphur estimated for planetary nebulae. Comparison between Figs. 7 and 8 clearly shows that the shape of sulfide particles is critical and one can easily imagine that an appropriate distribution of shapes could account for the 30 μm emission

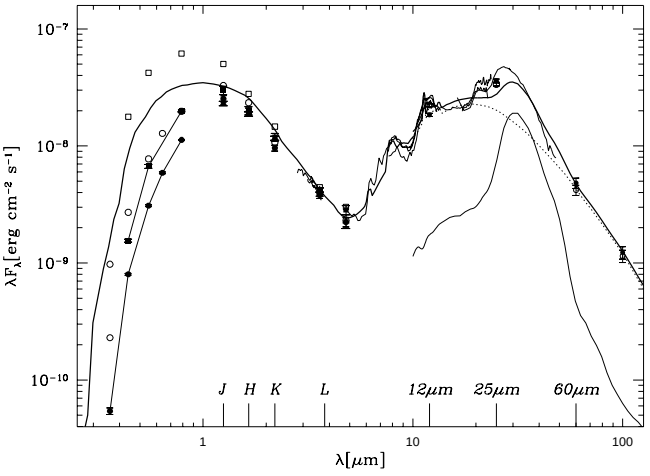

Fig. 8. The same as Fig. 7 but now for optical properties of sulfides obtained in CDE approximation.

band in IRAS 22272. On the other hand, unknown sulfide dust temperature prevents us from stating more definitely that they are responsible for the observed feature. Similar calculations performed assuming that the sulfide particles have the lowest possible dust temperature distribution predicted by our model gave fits of similar quality but required at the same time almost 4 times more sulphur (i.e. n(S)/n(H) = 1.6 10^{-5}), much more than the available abundance of S in PNe. Therefore, further laboratory measurements are necessary to estimate the short-wavelength absorption properties of MgS and in consequence to check whether this material could be responsible for the observed 30 μm feature.

Finally, to verify consistency of our model (which has been constructed by modeling of the spectral energy distribution) we compare its prediction with more detailed information about spatial distribution of emission at MIR wavelength. For this purpose we selected an image of IRAS 22272 at 11.8 μm obtained by Meixner et al. (1994). IRAS 22272 is resolved at this wavelength and has slightly elliptical structure with dimensions 2″ x 1.″8. To compare extension of emission at 11.8 μm with our 1D model we made a scan along the major axis of the image. In Fig. 9 we present normalized scan by means of open circles together with a gaussian of FWHM = 1″ representing the beam profile (dashed line). To get the model scan we convolved the model surface brightness at 11.8 μm with the appropriate circular gaussian beam. As can be seen in Fig. 9 the resulting spatial scan (solid line) matches reasonably well the extent of the emission at this wavelength.

5. Discussion

In the following we will discuss the implications of the parameters derived from the model fit to the energy distribution of IRAS 22272 (Fig. 4) which are listed in Table 1. Our attempt to find a fit to the energy distribution which lies in between the observed fluxes as corrected for different amounts of interstellar extinction (see Fig. 4 for details) showed that it is possible if

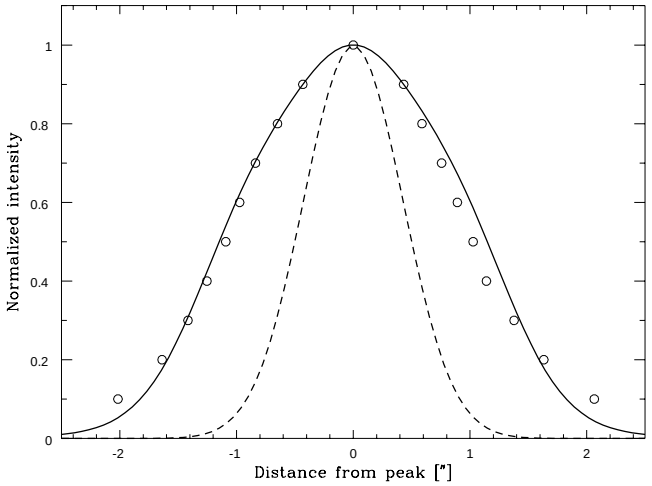

Fig. 9. Model fit (solid line) to the scan along major axis of IRAS 22272 (open circles) image at 11.8 μm. Dashed line represent gaussian beam profile with FWHM of 1″.

we assume a T_{eff} of about 5300 K for the star which radiates according to the model atmosphere calculations (the assumption of the black–body emission gave too much emission in UV part of the spectrum). If we assume a stellar temperature higher than $\approx$ 5500 K or lower than about 5000 K then we can obtain equally good fits in the IR range but the resulting models predict too much or too little energy emitted in the UV wavelengths respectively. At the same time a small adjustment (about 10 %) in distance (assuming constant stellar luminosity) is necessary. If we increased the assumed stellar temperature we had to adjust the fit by decreasing the assumed distance to the source slightly and vice versa if the assumed stellar temperature was decreased. This behaviour is a result of changes in wavelengths where maximum stellar flux is emitted for different effective temperatures. Our estimated effective temperature of about 5300 K agrees with a rough spectral classification of the source (Gp Ia – see Hrivnak & Kwok 1991), however it is slightly in disagreement with the more precise spectral class (G5 Ia) attributed to the source by Hrivnak (1995) which implies a central stellar temperature of about 4850 K (see Schmidt-Kaler 1982). With so low a central source temperature we were able to obtain a reasonable fit only to the short-wavelength observational data which were not corrected for interstellar extinction. Note, that Začs et al. (1995) got from the excitation analysis of their spectroscopic data for IRAS 22272 $T_{\rm eff} = 5600 \pm 250$ K in a good agreement with our estimate. It is possible that the effective temperature value for this star differs from that of a "real" G5 Ia star because IRAS 22272 presumably has an extremely low mass stellar envelope.

For modeling purposes, we adopted a stellar luminosity of 8318 $L_\odot$. For the distance derived from our fit ($d = 1.67$ kpc) we find that the total bolometric flux normalized to a distance of 1 kpc is 2982 $L_\odot$ (in a good agreement with results of van der Veen et al. 1989), while the IR flux (also normalized to 1 kpc) of 1470 $L_\odot$ agrees very well with the estimate of the total flux radiated in the IRAS wavelength range (1410 $L_\odot$) obtained from formula (1) of Loup et al. (1993).

Our assumed luminosity corresponds to a core mass of 0.64 $M_\odot$ on the basis of the core mass-luminosity relation (Wood & Zarro 1981). Comparison of the model parameters with the transition times presented in Table 1 of Górny et al. (1994) and based on the models of Schönberner (1979, 1983) and Blöcker & Schönberner (1990), suggests that the mass (and thus the luminosity) assumed for the central star of IRAS 22272 is rather too high. A strong argument against such a high mass comes from that the periods of radial pulsation for post-AGB objects are rather smaller than 100 days (Saselov 1984; Alcolea & Bujarrabal 1991) while for an assumed core mass of 0.64 $M_\odot$ the temperature of the star which would produce a fundamental pulsational period of 100 days is about 5250 K. The $T_{\rm eff}$ value from our model is very close to this value which could suggest, if we assume that the AGB stellar wind ceased when the stellar pulsation period was near 100 days, that during the last few hundred years ($t_{\rm dyn} = R_{\rm in}$(main shell)$/V_{\rm exp} = 750$ yr) the star has not had any change its temperature. However, this is in contradiction with the one-to-one relation between mass of the stellar envelope and star temperature for H-burning models during post-AGB phase of evolution (Schönberner, 1989). Nuclear burning itself, by reducing the mass of the envelope, is able to evolve the star to a temperature of about 5400 K from 5250 K during the estimated 750 yr period since the end of the AGB, but as we have shown we need some amount of hotter dust to obtain a good fit (if the estimated $1.35\,10^{-4}$ $M_\odot$ of gas in the hot dust component is removed from the stellar H-rich envelope the effective temperature is predicted to increase to about 6000 K from the post-AGB evolution models).

On the other hand, assuming that the mass of IRAS 22272 is equal to 0.60 $M_\odot$ the estimated distance to this source would be 14 % smaller (i.e. 1.45 kpc) and the dynamical age of the object would be reduced by approximately the same percentage to about 650 yr. If the large-scale mass loss (forming the main shell in our model) ended when the radial pulsation period dropped to a value of 100 days (when the stellar temperature reaches about 5000 K) then the derived age of 650 yr agrees with the transition times presented in Table 1 of Górny et al. (1994). The mass of the H-rich envelope predicted for this star at the end of the AGB phase is $1.175\,10^{-3}$ $M_\odot$. If we reduce this mass by our estimated mass of the hot dust shell ($1.35\,10^{-4}$ $M_\odot$) and in addition by the mass of H used for nuclear burning over the post-AGB time period ($5.43\,10^{-5}$ $M_\odot$) we estimate the mass of the remaining H-rich envelope to be $9.86\,10^{-4}$ $M_\odot$, which corresponds to a stellar effective temperature of 5370 K. This closely matches our estimate of 5300 K for the stellar effective temperature. Thus the parameters derived for IRAS 22272 are all consistent with a stellar mass of 0.60 $M_\odot$. We would like to mention that kinematic distance to the IRAS 22272 of 2.7 kpc (Woodsworth et al. 1990) seems to imply too high mass for the central star (about 0.89 $M_\odot$ on the basis of the core mass-luminosity relation of Wood & Zarro 1981 and obtained $L/d^2 = 2982\,L_\odot$). According to theoretical calculations (e.g. Blöcker 1995) star with such a high mass should evolve so fast that its effective temperature

cannot be still around 5000 K for the estimated dynamical time of post-AGB evolution of a few hundred years.

Of course, such an interpretation is only correct if central star of IRAS 22272 is generating its energy via hydrogen shell-burning. If the energy source is He shell-burning than the situation is more complicated as there is no unique relation between the mass of the envelope and the central star temperature according to the available models. IRAS 22272 has a C-rich envelope and if we take into account that all presently known Wolf-Rayet type stars (which are believed to be He-burners) among planetary nebula central stars are classified as C-type (they show carbon emission lines in their spectra, whereas the "regular" Wolf-Rayet stars which are thought to be much more massive are divided between C-type and N-type depending upon whether carbon or nitrogen emission lines are dominant in their spectra), there is a chance that at least some of the carbon-rich nebulae have central stars burning He rather than H at the base of their envelopes (but see Górny & Stasińska 1995 for a more detailed discussion). Unfortunately, we are not able to solve this problem with the present state of theory concerning H and He-burners.

We were not able to find a good fit to the IRAS 60 and 100 μm bands using amorphous carbon of AC type and a density distribution inversely proportional to the squared radius (which supposes a constant mass loss rate during AGB phase). Therefore we introduced a density distribution $\sim r^{-2.6}$ for the fit. Of course, different slopes of the dust opacity in the FIR will change slightly our results. Such an inferred density distribution for IRAS 22272 suggests that the mass loss rate increased during the formation of the circumstellar shell, from $\dot{M}^{\rm min}_{\rm AGB} \approx 4.70\,10^{-6}$ up to $\dot{M}^{\rm max}_{\rm AGB} \approx 5.76\,10^{-5}$ $M_\odot$ yr^{-1} (if we assume a dust-to-gas ratio equal to 0.005). Note, that gas mass loss rate estimated by Omont et al. (1993) from the measured CO line intensities (about $7.0\,10^{-6}$ $M_\odot$ yr^{-1} after scaling to the preferred by us distance to the IRAS 22272 of 1.45 kpc) is in agreement with our estimate as it is some type of mass-averaged value. From the best fit model we found that the required mass of dust necessary to explain the observed IR emission is about $2.3\,10^{-3}$ $M_\odot$.

While for AGB envelopes spherical symmetry seems to be typical, observations of post-AGB objects show that almost all of them are bipolar or have even more complicated structure. The reason for this and the moment when significant departure from the spherical symmetry inside ejected envelope took place is not clear. In principle, the easiest way to explain the shell asymmetry is to assume that most of the post-AGB objects evolve in binary systems (e.g. we can imagine that supergiant in IRAS 22272 has still undetected companion – maybe observations by International Ultroviolet Explorer could help test this possibility). On the other hand, an explanation which involves non-radial pulsations of late AGB star or its rotation are also plausible. In the context of aspherical shell structure, so typical for post-AGB evolution, it seems that for modeling of such sources anisotropic models could be more relevant. However, construction of such models is much more complicated and time consuming so their application to the larger group of objects is almost not possible at the moment. In the nearest future, we plan to apply some new method of the solution of the radiative transfer equation for axially-symmetric circumstellar dust disks (Men'shchikov & Henning 1996) to check how our conclusions in the case of IRAS 22272 depends on the possible anisotropies. Since degree of anisotropy in this object seems to be not so high (Trammell et al. 1994, Meixner at al. 1994) we can suspect that result should not be much different from that obtained by assumption of spherical symmetry. On the other hand, in the case of such objects as e.g. the Egg Nebula where anisotropy is really pronounced application of anisotropic models seems to be necessary.

6. Conclusions

One of the main aims of this study was to investigate what kind of dust is necessary to explain the unusual infrared spectrum observed from IRAS 22272+5435. We have found that PAHs (or molecules with very similar properties, e.g. hydrogenated solid amorphous carbon – see Buss et al. 1990) are essential for an interpretation of the spectral energy distribution. We also find that quantum treatment of their heating and cooling processes to be very important even for such a low temperature as 5300 K for the central star. It has been shown also that if the temperature of pure MgS-FeS grains is high enough we are able, in principle, to explain the observed 30 μm band by their IR emission, especially if we have a variety of shapes of grains inside the envelope. Until measurements of the absorption properties of MgS in the UV wavelengths become available, it will be rather difficult to rule out MgS as a possible carrier of the feature. On the other hand, sulfide mantles with amorphous carbon cores are found to be a less probable carrier of the feature as they possess two separate maxima with minimum around 30 μm in their absorption properties. The minimum disappears for thick coats, but this needs more sulphur than is available if coats are distributed proportionally to the surfaces of all AC grains present. Because the emitter(s) responsible for the 21 and 30 μm features are presently unknown, we have constructed an empirical opacity function which gave us a reasonable fit to the energy distribution between 18 and 48 μm.

The best fit constructed for IRAS 22272 allowed us to draw some conclusions concerning the evolutionary status of the source. We have shown that the estimated distance to this source is about 1.45 kpc if the mass of the central star is close to 0.60 $M_\odot$. The derived dynamical age of the nebula is then in agreement with the expected post-AGB evolution of such a hydrogen-burning star.

Acknowledgements. We would like to thank the anonymous referee who put our attention to the few aspects of this object which were not considered by us in the first version of the paper. Also we are very grateful to Margaret Meixner who kindly sent us her convolved image of IRAS 22272 at 11.8 μm and to Sascha Men'shchikov who provided us with his software helpful for the interpretation of the spatial information from our model. One of us (R.Sz.) express his gratitude to Canadian Institute of Theoretical Astrophysics and to Polish State Committee for Scientific Research – grant No. 2-2114-92-03.

References

Aller L.H., Czyzak S., 1983, ApJS 51, 211
Alcolea J., Bujarrabal V., 1991, A&A 245, 499
Begemann B., Dorschner B., Henning T., Mutschke H., 1994, ApJ 423, L71
Blöcker T., 1995, A&A 299, 755
Blöcker T., Schönberner D., 1990, A&A 241, L11
Bohren C.F., Huffman D.R., 1983, Absorption and Scattering of Light by Small Particles, John Wiley & Sons, Inc.
Bregman J.D., Allamandola L.J., Tielens A.G.G.M., Geballe T.R., Witteborn F.C., 1989, ApJ 344, 791
Buss R.H., Cohen M., Tielens A.G.G.M., Werner M., Bregman J.D. et al., 1990, ApJ 365, L23
Buss R.H., Tielens A.G.G.M., Cohen M., Werner M., Bregman J.D. et al., 1993, ApJ 415, 250
Bussoletti E., Colangeli L., Borghesi A., Orofino V., 1987 A&AS 70, 257
Cardelli J.A., Clayton G.C., Mathis J.S., 1989, ApJ 345, 245
Cox P., 1993, Far-Infrared Spectroscopy of Solid State Features. In: Kwok S. (ed) Astronomical Infrared Spectroscopy: Future Observational Directions. ASP Conf. Ser. 41, p. 163
Desert F.-X., Boulanger F., Puget J.L., 1990, A&A 237, 215
Dominik C., Sedlmayr E., Gail H.-P. 1993, A&A 277, 578
Egan M.P., Leung C.M., Spagna G.F., 1978, Comp. Physics Communications 48, 271
Geballe T.R., Tielens A.G.G.M., Kwok S., Hrivnak B.J., 1992, ApJ 387, L89
Goebel J.H., Moseley S.H., 1985, ApJ 290, L35
Górny S.K., Tylenda R., Szczerba R.: 1994, A&A 284, 949
Górny S.K., Stasińska G., 1995, A&A 303, 893
Guhathakurta P., Draine B.T., 1989, ApJ 345, 230
Justtanont K., Barlow M.J., Skinner C.J., Roche P.F., Aitken D.K., Smith C.H., 1996, A&A 309, 612
Henning Th., Chan S.J., Assendorp R., 1996, A&A 312, 511
Hrivnak B.J., 1995, ApJ 438, 341
Hrivnak B.J., Kwok S., 1991, ApJ 371, 631
Jura M., 1994, ApJ 43, 713
Kwok S., Volk K., Hrivnak B.J., 1989, ApJ 360, L23
Kwok S., Hrivnak, B.J., Milone E.F., 1986, ApJ 303, 451
Kwok S., Hrivnak B.J., Geballe Th. R., 1995, ApJ 454, 394
Laor A., Draine B.T., 1993, ApJ 402, 441
Leung C.M., 1975, ApJ 199, 340
Leung C.M., 1976, ApJ 209, 75
Lindqvist M., Nyman L.-A., Olofsson H., Winnberg A., 1988, A&A 205, L15
Loup C., Forveille Th., Omont A., Paul J.F., 1993, A&AS 99, 291
Manchado A., Pottasch S.R., Garcia-Lario P., Esteban C., Mampaso A., 1989, A&A 214, 139
Mathis J.S., Rumpl W., Nordsieck K.H., 1977, ApJ 217, 425
Meixner M., Graham J.R., Skinner C.J., Hawkins G.W., Keto E., et al., 1994, Mid-IR (8-13 μm) Images of the 21 μm Carbon Rich Proto-Planetary Nebulae. In: Experimental Astronomy, Vol. 3, Nos. 1–4, 53
Men'shchikov A.B., Henning Th., 1996, A&A submitted
Neckel Th., Klare G., 1980, A&AS 42, 251
Nuth J.A., Moseley S.H., Silverberg R.F., Goebel J.H., Moore W.J., 1985, ApJ 290, L41
Omont A., 1993, Circumstellar Matter: Cool IRAS Sources. In: Kwok S. (ed) Astronomical Infrared Spectroscopy: Future Observational Directions. ASP Conf. Ser. 41, p. 87
Omont A., Loup C., Forveille T., te Lintel Hekkert P., Habing H., et al., 1993, A&A 267, 515
Omont A., Cox P., Moseley H.S., Glaccum W., Casey S., et al., 1995a, Mid- and Far-Infrared Emission Bands in C-rich Proto-planetary Nebulae. In: Haas M.R., Davidson J.A., Erickson E.F. (eds) Astronomical Society of the Pacific, Airborne Astronomy Symposium on the Galactic Ecosystem: From Gas to Stars to Dust, vol. 73, p. 413
Omont A., Moseley H.S., Cox P., Glaccum W., Casey S., et al., 1995b, ApJ 454, 819
Pottasch S.R., Parthasarathy M., 1988, A&A 192, 182
Rouleau F., Martin P.G., 1991, ApJ 377, 526
Saselov D.D., 1984, Ap&SS 102, 161
Schmidt-Kaler Th, 1982, Physical parameters of the stars. In: Schaifers K., Voigt M.H. (eds.) Landolt Börnstein A&A Vol. VI, 2b. Springer, Berlin, p. 451
Schönberner D., 1979, A&A 79, 108
Schönberner D., 1983, ApJ 272, 708
Schönberner D., 1989, Evolutionary tracks for central stars of planetary nebulae, In: Torres-Peimbert S. (ed) IAU Symposium 131: Planetary Nebulae. Kluwer Academic Publishers, Dordrecht/Boston/London
Schutte W.A., Tielens A.G.G.M., Allamandola L.J., 1993, ApJ 415, 397
Siebenmorgen R., Krügel E., 1992, A&A 259, 614
Siebenmorgen R., Krügel E., Mathis J.S., 1992, A&A 266, 501
Szczerba R., et al. 1996a in preparation
Szczerba R., Volk K., Kwok S., 1996b Dust Around post-AGB Sources with 21 μm Feature. In: Siebenmorgen R., Käufl U. (eds) ESO Workshop: The Role of Dust in Formation of Stars. in press
Trammell S.R., Dinerstein H.L., Goodrich R.W., 1994, AJ 108, 984
van der Veen W.E.C.J., Habing H.J., Geballe T.R., 1989, A&A 226, 108
Volk K., Kwok S., Stencel R., Brugel E., 1991, ApJS 77, 607
Walmsley C.M., Chini R., Kreysa E., Steppe H., Forveille T., et al., 1991 ApJ 248, 555
Wood P.R., Zarro D.M., 1981, ApJ 247, 247
Woodsworth A., Kwok S., Chan S.J., 1990, A&A 228, 503
Yorke H.W., 1980a, A&A 85, 215
Yorke H.W., 1980b, A&A 86, 286
Zuckerman B., Dyck H.M., Claussen M.J., 1986, ApJ 304, 401
Začs L., Klochkova V.G., Panchuk V.E., 1995, MNRAS 275, 764

This article was processed by the author using Springer-Verlag LaTeX A&A style file *L-AA* version 3.